Sensors and Actuators A 211 (2014) 67–77

Contents lists available at ScienceDirect

Sensors and Actuators A: Physical

journal homepage: www.elsevier.com/locate/sna

High-performance trajectory tracking control of a quadrotor with disturbance observer

Wei Dong, Guo-Ying Gu*, Xiangyang Zhu, Han Ding

State Key Laboratory of Mechanical System and Vibration, Shanghai Jiao Tong University, Shanghai 200240, China

ARTICLE INFO

Article history:
Received 1 January 2014
Received in revised form 6 March 2014
Accepted 6 March 2014
Available online 15 March 2014

Keywords:
Quadrotor
Backstepping
Trajectory tracking control
Disturbance observer

ABSTRACT

In this paper, a flight controller with disturbance observer (DOB) is proposed for high-performance trajectory tracking of a quadrotor. The dynamic model of the quadrotor, considering the external disturbances, model mismatches and input delays, is firstly developed. Subsequently, a DOB-based control strategy is designed with the backstepping (BS) technique. In this control scheme, the DOB serves as a compensator, which can effectively reject model mismatches and external disturbances. In this case, the trajectory tracking controller is designed according to the nominal model. Then, the input-to-state stability (ISS) analyses of the developed controllers are presented, which theoretically guarantees the robustness of the developed controller. Finally, comparative studies are carried out. Three types of disturbances including payloads, rotor failures and wind are chosen to verify the effectiveness of the development. The results from simulations and experiments show that the proposed controller provides better performances than the traditional nonlinear controllers.

1. Introduction

Over the recent years, the quadrotors, a kind of unmanned aerial vehicles (UAV), attract more and more attentions in the robotics community [1]. With their small size and agile maneuverability, the quadrotors provide mobilities which cannot be covered by humans, for instance, in cluttered or dangerous environments where the human being is at risk [2,3]. These capabilities of quadrotors allow to cope with a diverse scenarios imposed by real-world missions [4], such as photography, traffic monitoring, reconnaissance, homeland security, damage assessment, etc. [5].

In these missions, the performance of the quadrotors implicitly depends on the flight controllers. Therefore, high-performance controllers are essential and many researchers have involved themselves into this field. Bouabdallah et al. firstly developed a group of classical controllers, including the proportional-integral-derivative (PID) controller, linear quadratic (LQ) controller [6], backstepping controller and sliding-mode controller [7]. These controllers solve the basic problems of flight control and some of them are still widely adopted nowadays [8,1]. Later, for the purpose of robust control, modern control theories were implemented in the controller design, such as Lyapunov function design method [9] and hierarchy theory [10]. The effectiveness of these controllers were verified theoretically and experimentally. However, no evidence shows these controllers can handle external disturbances and model mismatches, such as payloads, wind and rotor damages. This drawback obviously deteriorates the performance of the flight controllers. Therefore, more reliable and robust controllers are necessary. To this end, several groups have made efforts to develop controllers that are capable of disturbance rejection. A representative development is a so called composite model reference adaptive controller developed by Dydek et al. [11]. This controller was verified to be capable of dealing with rotor failures in an experiment of altitude control. In [4,12–14], adaptive controllers of different structures were also verified by simulations and experiments on ground stations. Alternatively, the DOB-based controller is robust to external disturbances and model mismatches without the use of high control gain or extensive computational power [15]. The DOB provides a feasible approach to estimate disturbances while relying only on knowledge of the nominal model and limits of the disturbances [15,16].With the introduction of DOB, the controller can then be developed based on traditional methods. Comparing to the adaptive control, the DOB makes the controller design more flexible and reduces the complexities [17]. Besnard et al. firstly adopted sliding mode disturbance observer for robust controller design [15,18,19]. Later, different kinds of DOB-based controllers

* Corresponding author. Tel.: +86 21 34206108.
E-mail addresses: chengquess@sjtu.edu.cn (W. Dong), guguoying@sjtu.edu.cn, guguoying@gmail.com (G.-Y. Gu), mexyzhu@sjtu.edu.cn (X. Zhu), hding@sjtu.edu.cn (H. Ding).

http://dx.doi.org/10.1016/j.sna.2014.03.011
0924-4247/

were developed for disturbance rejection in attitude control and 2D trajectory tracking [20–23].

Results from these works show the potential capabilities of DOB-based controllers for handling external disturbances and model mismatches, such as wind and actuator failure [15]. However, none of them is developed for the purpose of trajectory tracking of a quadrotor in real time. Therefore, this work is motivated to develop a high-performance DOB-based controller with experimental studies. Firstly, in order to develop an effective model for the controller design, the dynamic behaviors of the quadrotor are further studied by considering external disturbances, model mismatches and input delays. Subsequently, the DOB is designed and an integral filter is introduced to alleviate the effects of input delays and high frequency noises. In this way, the filter's output can be viewed as the estimate of the lumped disturbance. By subtracting this estimate, the major disturbances, especially low-frequency disturbances, can be eliminated. In such a case, a control scheme for trajectory tracking can be developed according to the nominal model. In this control scheme, the position error is stabilized by a proportional-integral (PI) controller, and the velocity error is stabilized by a BS controller. The stability analysis is then provided to theoretically confirm the robustness of the developed controllers. Finally, experiments are carried out to verify the development.

The contribution of this paper lies in two aspects. Firstly, to get a better understanding of the quadrotor's dynamic behavior, a mathematical model, which considering the external disturbances, model mismatches and input delays, is developed. Secondly, a high-performance DOB-based backstepping controller is developed and experimentally verified for the real-time trajectory tracking of the quadrotor. This controller can cope with wind, varying payloads and rotor failures. To the best knowledge of the authors, no such controller has been adopted in the real time trajectory tracking of a quadrotor.

The remainder of this paper is organized as follows. Section 2 proposes the dynamic model of the quadrotor. The DOB-based controller is designed in Section 3, and the stability analysis is provided in Section 4. Then the results from simulation and experiments are shown in Section 5, and Section 6 concludes this work.

2. Quadrotor model and problem statement

To facilitate the controller design, the dynamic model of the quadrotor is developed in this section. In this model, external disturbances, input delays and model mismatches are considered as the lumped disturbance which will be handled by the following developed controller.

2.1. Quadrotor dynamics

As shown in Fig. 1, the quadrotor is actuated by four rotors on the endpoints of an X-shaped frame. The collective thrust of these four rotors accelerates the quadrotor along its normal direction (Z_B). In order to balance the yawing torque, rotors attached on the Y_B axis rotate in clockwise direction, and the rotors attached on the X_B axis rotate in counterclockwise direction. As a result, the difference of collective torques between these two axes produces a yawing torque. Similarly, differences of thrusts between rotors on the X_B axis and Y_B axis produce a pitching torque and a rolling torque respectively. Therefore, four control inputs can be defined as

$$\begin{cases} U_1 = F_1 + F_2 + F_3 + F_4 \\ U_2 = (F_4 - F_2)L \\ U_3 = (F_3 - F_1)L \\ U_4 = M_1 - M_2 + M_3 - M_4 \end{cases} \tag{1}$$

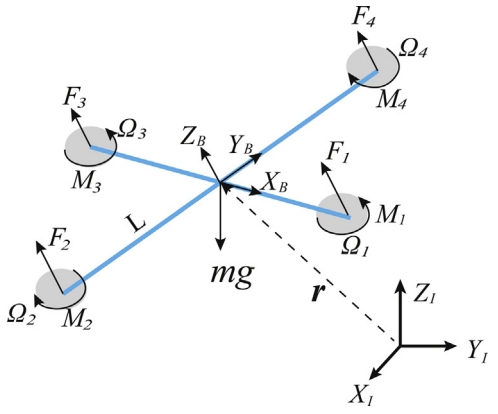

Fig. 1. A depict for the quadrotor. $X_I - Y_I - Z_I$ is the inertial coordinates and $X_B - Y_B - Z_B$ is the body fixed coordinates.

where L is the length from the rotor to the center of the mass of the quadrotor, F_i is the generated thrust, and M_i is the generated torque.

The thrusts and torques can be obtained by varying the rotary speeds of the rotors. This relations are commonly estimated by [24,25,1]

$$F_i = k_F \frac{\omega_F}{s + \omega_F} \Omega_{id}, \quad M_i = k_M \frac{\omega_M}{s + \omega_M} \Omega_{id} \tag{2}$$

where k_F, k_M, ω_F, ω_M are constants related to the rotor, and Ω_{id} is the reference for the speed of the rotor.

In view of (1) and (2), the rigid body dynamics using Newton–Euler formalism is governed

$$\begin{cases} m\ddot{\boldsymbol{r}} = U_1 \boldsymbol{Z}_B - mg\boldsymbol{Z}_I - \boldsymbol{k} \circ \dot{\boldsymbol{r}} \circ |\dot{\boldsymbol{r}}| \\ \boldsymbol{I}\ddot{\boldsymbol{q}} = \begin{bmatrix} U_2 & U_3 & U_4 \end{bmatrix}^T - \dot{\boldsymbol{q}} \times \boldsymbol{I}\dot{\boldsymbol{q}} \end{cases} \tag{3}$$

where m is mass of the quadrotor, g is the local gravity constant, $\boldsymbol{r}$ is the position in inertia frame with $\boldsymbol{r} = [x, y, z]^T$, $\boldsymbol{q}$ is the attitude in body frame with $\boldsymbol{q} = [\phi, \theta, \psi]^T$, $\boldsymbol{I}$ is the rotary inertia, $\boldsymbol{k}$ is a constant to estimate the aerial drag effects, and the symbol $\circ$ denotes the element-wise product.

Since the rotary inertia is small and the quadrotor is symmetric, the term $\dot{\boldsymbol{q}} \times \boldsymbol{I}\dot{\boldsymbol{q}}$ is small and insignificant [1,26,7,11,27]. Therefore, (3) can be reduced into

$$\begin{cases} \ddot{x} = \dfrac{1}{m}(U_1(\cos\phi \sin\theta \cos\psi + \sin\phi \sin\psi) - k_x \dot{x}|\dot{x}|) \\ \ddot{y} = \dfrac{1}{m}(U_1(\cos\phi \sin\theta \sin\psi - \sin\phi \cos\psi) - k_y \dot{y}|\dot{y}|) \\ \ddot{z} = \dfrac{1}{m}(U_1(\cos\phi \cos\theta) - k_z \dot{z}|\dot{z}| - mg) \\ \ddot{\phi} = \dfrac{U_2}{I_{xx}} \\ \ddot{\theta} = \dfrac{U_3}{I_{yy}} \\ \ddot{\psi} = \dfrac{U_4}{I_{zz}} \end{cases} \tag{4}$$

where I_{xx}, I_{yy}, and I_{zz} are the rotary inertia of the quadrotor respect to the X_B, Y_B, and Z_B axis.

2.2. Problem statement

Traditional controllers, such as PID controller, LQ controller [6] and sliding-mode controller [7], for trajectory tracking are commonly developed based on (4) [1,24,25]. However, as uncertainties may arise in (4), these controllers inherently lack of the capabilities

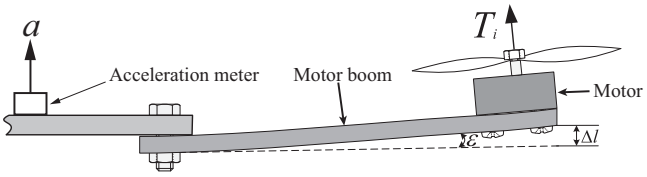

Fig. 2. Due to the structural distortion, a transport delay occurs between the generated thrust and the measured acceleration.

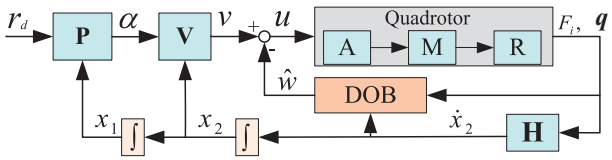

Fig. 3. The structure of control system for the quadrotor.

of disturbance rejection. Therefore, in order to develop disturbance rejection controllers, the dynamic model should be firstly improved by including the dynamics of these uncertainties. In the trajectory tracking control of the quadrotors, the major sources of uncertainties are external disturbances, modeling mismatches and input delays [11,18]. In particular, the input delays, which are commonly neglected in other works [28], are caused by the transport delay in inner control loop and structural distortion. As indicated in Fig. 2, when the thrust T_i is generated by the motor according to the command of the inner loop controller, the elastic distortion ε occurs on the motor boom due to the non-ideal rigid structure of the airframe. As a result, the acceleration a in the center of the quadrotor can only be measured by the acceleration meter after the motor accelerates for some distance Δl. In addition, the dynamics of the motor itself cannot be instantaneously reached. Therefore, extra attention should be paid to deal with the effects of the input delays.

By taking these described uncertainties into account, the dynamic model for the trajectory can be rewritten in the form

$$\begin{cases} \dot{x}_1 = x_2 \\ \dot{x}_2 = F(\boldsymbol{x}) + G(\boldsymbol{x})u(t-\tau_r) + d(\boldsymbol{x}, t) \end{cases} \tag{5}$$

where $\boldsymbol{x} = [x_1, x_2]^T$, x_1 and x_2 are the position and velocity of the quadrotor, with $x_1 = [x, y, z]^T$; $F(\boldsymbol{x})$ and $G(\boldsymbol{x})$ are modelable nonlinear functions; $d(x, t)$ is an unknown function representing the external disturbances and other unmodeled nonlinearities; τ_r represents the input delay.

As there is no way to obtain precise forms of $F(\boldsymbol{x})$ and $G(\boldsymbol{x})$, a nominal model, such as (4), is commonly adopted for controller design. Denoting the nominal model as $F_0(\boldsymbol{x})$ and $G_0(\boldsymbol{x})$, $F(\boldsymbol{x})$ and $G(\boldsymbol{x})$ can be expressed as

$$F(\boldsymbol{x}) = F_0(\boldsymbol{x}) + \Delta_F(\boldsymbol{x}), \quad G(\boldsymbol{x}) = G_0(\boldsymbol{x}) + \Delta_G(\boldsymbol{x}) \tag{6}$$

where $\Delta_F(\boldsymbol{x})$ and $\Delta_G(\boldsymbol{x})$ are modeling errors.

Considering boundaries of the system, two assumptions are made for the following controller design.

Assumption 1. $G_0(\boldsymbol{x})$ and $G(\boldsymbol{x})$ have the same sign and are bounded away from zero.

Assumption 2. There exist finite positive constants M_F, M_d, M_{F_0}, M_G, $M_{\Delta G} < \infty$ and continuous functions $\bar{F}(\boldsymbol{x})$ and $\bar{d}(\boldsymbol{x})$ which satisfy the following inequalities:

$$\frac{|\Delta_F(\boldsymbol{x})|}{\bar{F}(\boldsymbol{x})} \le M_F, \quad \frac{|d(\boldsymbol{x})|}{\bar{d}(\boldsymbol{x}, t)} \le M_d, \quad \frac{|F_0(\boldsymbol{x})|}{\bar{F}(\boldsymbol{x})} \le M_{F_0} \tag{7}$$

$$\frac{G_0(\boldsymbol{x})}{G(\boldsymbol{x})} \le M_G, \quad \left|\frac{\Delta_G(\boldsymbol{x})}{G(\boldsymbol{x})}\right| \le M_{\Delta G} \tag{8}$$

Remark 1. Assumption 1 implies the mathematic modeling is reliable, and there is no chance to produce an infinite control input. Assumption 2 implies the disturbances and modeling errors dealt in this work are bounded.

3. DOB-based controller design

In this section, we aim to design a trajectory tracking control strategy which can effectively compensate for the lumped disturbance.

As shown in Fig. 3, this control scheme is developed in a cascaded structure, which means the attitude controller works as the inner loop controller of the trajectory tracking controller. With such a scheme, the quadrotor is stabilized in the following way. The quadrotor dynamics is governed by **R** and **H**, which is expressed in (4) and (5). The control inputs U_i ($i = 1, 2, 3, 4$) for **R** are generated by rotors which have their own dynamics **M** as in (2). The controller **A** is designed to control the attitude $\boldsymbol{q}$ through U_2, U_3 and U_4. Taking $\boldsymbol{q}$ and U_1 as the control inputs, the trajectory tracking control is realized by a position controller **P** and a velocity controller **V**.

Based on such a structure, this section designs a DOB-based control strategy for trajectory tracking. As the attitude is the input for this control scheme, an attitude controller serving as an inner loop is developed at the end of this section.

3.1. Trajectory tracking control

When the quadrotor takes flights near the hovering state ($\phi \approx 0$, $\theta \approx 0$), (4) can be linearized as

$$\begin{cases} \ddot{x} = \dfrac{1}{m}(U_1(\theta\cos\psi + \phi\sin\psi) - k_{x_0}\dot{x}|\dot{x}|) \\ \ddot{y} = \dfrac{1}{m}(U_1(\theta\sin\psi - \phi\cos\psi) - k_{y_0}\dot{y}|\dot{y}|) \\ \ddot{z} = \dfrac{1}{m}(U_1\cos\phi\cos\theta - k_{z_0}\dot{z}|\dot{z}| - mg) \end{cases} \tag{9}$$

Therefore, the nominal expressions of $F(\boldsymbol{x})$ and $G(\boldsymbol{x})$ are

$$F_0(\boldsymbol{x}) = \frac{-1}{m}\left[k_x\dot{x}|\dot{x}|, \quad k_y\dot{y}|\dot{y}|, \quad k_z\dot{z}|\dot{z} + mg\right]^T \tag{10}$$

$$G_0(\boldsymbol{x}) = \frac{1}{m}\begin{bmatrix} U_1\cos\psi & U_1\sin\psi & 0 \\ U_1\sin\psi & -U_1\cos\psi & 0 \\ 0 & 0 & \cos\phi\cos\theta \end{bmatrix} \tag{11}$$

The input vector for the trajectory tracking control is then defined as

$$u = \left[\theta, \quad \phi, \quad U_1\right]^T \tag{12}$$

With (5), (6), and (10)–(12), the controller for trajectory tracking is designed as follows.

Firstly, the position error signal and velocity error signal are defined as

$$z_1 = x_1 - y_r, \quad z_2 = x_2 - \alpha_1 \tag{13}$$

where y_r is the reference for the position, and α_1 is the virtual input to stabilize z_1.

According to (5), a subsystem $\mathcal{S}_1$ representing the position loop can be defined as

$$\mathcal{S}_1: \quad \dot{z}_1 = \alpha_1 + z_2 - \dot{y}_r \tag{14}$$

This virtual input α_1 is designed based on the common PI control algorithm

$$\alpha_1 = -c_{1p}z_1 - c_{1i}\int_0^t z_1 dt + \dot{y}_r \tag{15}$$

where $c_{1p} > 0$, $c_{1i} > 0$. Differentiating (15) gives

$$\dot{\alpha}_1 = -c_{1p}\dot{z}_1 - c_{1i}z_1 + \ddot{y}_r = -c_{1p}(x_2 - \dot{y}_r) - c_{1i}z_1 + \ddot{y}_r \tag{16}$$

Then, according to (5), (6) and (13), the subsystem $\mathcal{S}_2$ representing the velocity loop is defined as

$$\mathcal{S}_2 : \dot{z}_2 = F_0(\boldsymbol{x}) + G_0(\boldsymbol{x})u - \dot{\alpha}_1 + d(\boldsymbol{x}, t) + \Delta_F(\boldsymbol{x}) + \Delta_G(\boldsymbol{x})u \tag{17}$$

This velocity error z_2 is stabilized as follows. According to (5), the lumped disturbance is

$$w = d(x, t) + \Delta_F(\boldsymbol{x}) + \Delta_G(\boldsymbol{x})u(t-\tau) = \dot{z}_2 - (F_0(\boldsymbol{x}) + G_0(\boldsymbol{x})u(t) - \dot{\alpha}_1) \tag{18}$$

The compensation term for the input can be then calculated as $\hat{w} = w/G_0(\boldsymbol{x})$. When the inverse of the nominal model $1/G_0(\boldsymbol{x})$ is noncausal and high frequency noises exist, a low pass filter, usually called Q-filter, is commonly required [29]. With the relative degree larger than or equal to the relative degree of the nominal model, the Q-filter enables the DOB practical implementable and filters out the noises. In this work, as the nominal model $G_0(\boldsymbol{x})$ is approximately a constant matrix and nontrivial near the hovering state, the causality problem doesn't exist. Furthermore, there are the small but time varying input delays. These input delays might vary as high as several times of the sampling time, so it is impractical to eliminate their effects by simply replacing $G_0(\boldsymbol{x})u(t)$ with $G_0(\boldsymbol{x})u(t-\tau)$ in (18). To this end, an integral filter is designed to tackle the input delays as follows

$$\tilde{w} = \frac{z_2 + \alpha_1 - \int_0^t (F_0(\boldsymbol{x}) + G_0(\boldsymbol{x})u)dt}{t} \tag{19}$$

In such a case, the DOB is developed. Then replacing u in (17) by $u = (\hat{v} - F_0(\boldsymbol{x}) + \dot{\alpha}_1 - \tilde{w})/G_0(\boldsymbol{x})$ and assuming $\tilde{w} \approx w$, the following simple nominal model can be obtained

$$\dot{z_2} \simeq \hat{v} \tag{20}$$

where $\hat{v}$ is a nominal linear input.

This indicates that an inner-loop for acceleration control is formed such that the inner-loop approximates the nominal model as described in (9). Therefore, a traditional controller can be adopted according to the nominal model. In this work, a linear input is chosen as $\hat{v} = -c_2 z_2$. Then the input u is obtained as

$$u = \frac{-c_2 z_2 + \dot{\alpha}_1 - F_0(\boldsymbol{x}) - \tilde{w}}{G_0(\boldsymbol{x})} \tag{21}$$

where $v = (-c_2 z_2 + \dot{\alpha}_1 - F_0(\boldsymbol{x}))/(G_0(\boldsymbol{x}))$ is the input generated by the velocity controller.

When the quadrotor stays at ground, the disturbances estimated by $\tilde{w}$ is meaningless and the integration action in $\tilde{w}$ may increase infinitely. To avoid this drawback, a saturation boundary is introduced such that

$$|\tilde{w}| \le M_w \tag{22}$$

Remark 2. This M_w also affects the performance of the controller. Theoretically, any positive constant less than the dynamic boundary of the quadrotor, namely $\sup(U_1/m)$, is a candidate. However, if its value is too large, it will take long time for the controller to stabilize from a fault estimation, but if the value is too small, the controller cannot compensate large disturbances.

As all of the disturbances or model mismatches interested by this work are at very low frequencies, one can expect $\tilde{w} \approx w$. High frequency disturbances such as noises in measurement are filtered out by the integration in $\tilde{w}$. With this development, it can be concluded that $\tilde{w}$ can make good estimation for the external disturbances and modeling errors. When compensated by $\tilde{w}$, z_2 can be asymptotically stabilized to zero even if disturbances arise, which shall be analyzed in the next section.

3.2. Attitude control

According to (12), ϕ and θ are two control inputs for the trajectory tracking. Therefore, it is necessary to stabilize the attitude with an inner loop controller. Based on (4), an attitude controller is developed as follows.

Firstly, the angular error signal and rotary rate error signal are defined as

$$z_{a1} = q - q_d, \quad z_{a2} = \dot{q} - \alpha_{a1} \tag{23}$$

where q_d is the desired attitude, q is the measured attitude, and α_{a1} is a virtual input to stabilize z_{a1}.

The attitude controller is then designed as

$$u_a \simeq \dot{z}_{a2} = -k_r z_2, \quad \alpha_{a1} = -k_a z_1 \tag{24}$$

where k_r and k_a are positive number, and $u_a = [U_2, U_3, U_4]^T$.

It can be seen that the desired values of control inputs U_i ($i = 1, 2, 3, 4$) have been generated by the trajectory tracking controller and the attitude controller. As the actual values of U_i might be not exactly the same as the desired values in the real-time flights, these desired values are denoted as U_{id} in the following development. Subsequently, one can calculate the RPM command for each rotor by using (1) and (2)

$$\begin{bmatrix} \Omega_{1d} \\ \Omega_{2d} \\ \Omega_{3d} \\ \Omega_{4d} \end{bmatrix} = \begin{bmatrix} k_T & 0 & k_{\phi\theta} & k_\psi \\ k_T & -k_{\phi\theta} & 0 & -k_\psi \\ k_T & 0 & -k_{\phi\theta} & k_\psi \\ k_T & k_{\phi\theta} & 0 & -k_\psi \end{bmatrix} \begin{bmatrix} U_{1d} \\ U_{2d} \\ U_{3d} \\ U_{4d} \end{bmatrix} \tag{25}$$

where k_T, $k_{\phi\theta}$ and k_ψ are constants related to the parameters of the model.

4. Stability analysis

This analysis focuses on the trajectory tracking control.

Substituting (15) into $\mathcal{S}_1$, one can obtain

$$\dot{z}_1 = z_2 - c_{1p}z_1 - c_{1i}\int_0^t z_1 dt \tag{26}$$

Eq. (26) can be rewritten into the state-space form

$$\dot{z}_{1a} = \boldsymbol{A}z_{1a} + \boldsymbol{B}z_2 \tag{27}$$

where

$$z_{1a} = \left[\int_0^t z_1 dt, z_1\right]^T, \quad \boldsymbol{A} = \begin{bmatrix} 0 & 1 \\ -c_{1i} & -c_{1p} \end{bmatrix}, \quad \boldsymbol{B} = \begin{bmatrix} 0 & 1 \end{bmatrix}^T \tag{28}$$

The ISS property of the subsystem $\mathcal{S}_1$ can be guaranteed by in the following lemma [30,31].

Lemma 1. *If the virtual input α_1 is applied to subsystem $\mathcal{S}_1$ and if z_2 is made uniformly bounded, $\mathcal{S}_1$ is ISS, i.e., for $^\exists\lambda_0 > 0$, $^\exists\rho_0 > 0$*

$$|z_{1a}(t)| \le \lambda_0 e^{-\rho_0 t}|z_{1a}(0)| + \frac{\lambda_0}{\rho_0}\left[\sup_{0\le\tau\le t}|z_2(\tau)|\right] \tag{29}$$

Therefore, it is necessary to prove the boundedness of z_2, and this can be analyzed as follows.

Applying the designed control input u to the subsystem $\mathcal{S}_2$, one can have

$$\dot{z}_2 = -c_2 z_2 + w - \tilde{w} \tag{30}$$

The solution of (30) is in the form

$$z_2 = C_z e^{-c_2 t} + e^{-c_2 t} \int_0^{\tau} (w - \tilde{w}) e^{c_2 \tau} d\tau \tag{31}$$

According to (7), (8) and (22), $w - \tilde{w}$ is bounded. Hence

$$|z_2(t)| \le \beta_1 |z_2(0)| e^{-\beta_0 t} + \beta_2 \sup_{0 \le \tau \le t} |w - \tilde{w}| \tag{32}$$

where $\beta_i > 0$.

Thus, the stabilities of the overall system are guaranteed according (29) and (32).

5. Simulations and experiments

In this section, extensive simulations and experiments are carried out to demonstrate the effectiveness of the proposed control strategy.

5.1. System identification and parameter selecting

To verify previous formulations and obtain further understanding for the quadrotor, experiments are carried out to identify the parameters of the quadrotor model firstly. Based on the results of the identification, control gains are then selected for the developed controllers.

5.1.1. Attitude control

According to (1), (2), (4) and (25), it is necessary to identify the parameters of the rotor and the quadrotor airframe prior to the attitude controller design.

The identification for the rotor is carried out on a specially designed test bench. As shown in Fig. 4, one rotor from the quadrotor is set up on a stress sensor (model YP-L1, Yeepo Automation) and a torque sensor (model YP-NJ, Yeepo Automation). The stress sensor is capable of measuring the stress from 0 N to 50 N with a tolerance of 0.02%, and the torque sensor is capable of measuring the torque from 0 N m to 5 N m with a tolerance of 0.3%. As the electrical signals from these sensors are very small, a transducer (model YP-FD, Yeepo Automation) is implemented to convert them into 0–5 V voltage signals. The converted voltage signals are then sampled by a data acquisition (model USB-6363, National Instrument) at a frequency of 1000 Hz. Finally, these sampled data are collected via a program written in Labview.

With this developed test bench, the rotor is controlled by an onboard program which generates RPM commands according to users' instruction. In this work, the commands are specified to rise from 10% to 80% of the full speed of the rotor (8000 RPM) by an increment of 10% at each step. For each speed, the generated thrust/torque is measured for 10 s.

The results are shown in Fig. 5. It is interesting to see that the rotor does not behave exactly as the theoretical prediction in aerodynamics [32], where the thrust/moment is quadratically related to the speed of the rotor as

$$F_i = k_f \Omega_i^2, \quad M_i = k_m \Omega_i^2 \tag{33}$$

where k_f and k_m are parameters related to the rotor, and Ω_i is the speed of the rotor.

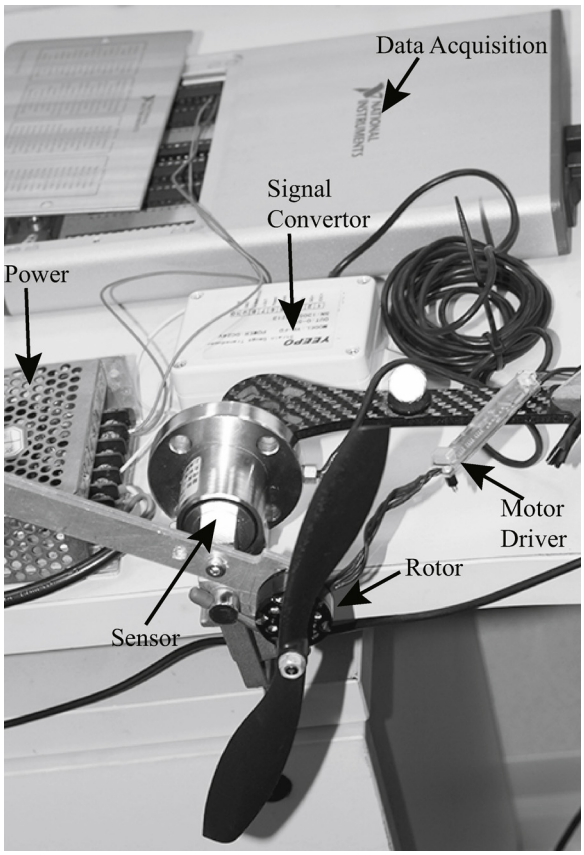

Fig. 4. A test bench designed to identify the parameters of the rotor.

The results from data fitting show that the relation between thrust and speed of the rotor can be estimated by

$$y = 2.56 \times 10^{-5} x^{1.37} \tag{34}$$

Similarly, the relation between torque and speed of the rotor can be estimated by

$$y = 1.20 \times 10^{-6} x^{1.25} \tag{35}$$

From (34) and (35), it is reasonable to estimate the motor dynamics by a linear equation as in (2).

The inertia of the quadrotor is then measured by a three wire pendulum [33], and the mass is measured by an electronic balance. These identified parameters of the quadrotor are shown in Table 1. From these results, one can obtain

$$\frac{1}{I_{xx}} \approx \frac{1}{I_{yy}} \approx \frac{1}{I_{zz}} \approx 100 \frac{1}{m} \tag{36}$$

In practice, it is more convenient to scale the control inputs U_{id} in (21) and (24) into a same range, which will make the controller design easier. For this purpose, according to (4) and (36), the parameters in (25) should satisfy the relation $k_{\phi\theta} = k_{\psi} = k_T/100$.

Table 1
The identified parameters of the quadrotor

Item	Quantity
L (m)	0.2
m (kg)	0.547
I_{xx} (kg.m^2)	0.0033
I_{yy} (kg.m^2)	0.0033
I_{zz} (kg.m^2)	0.0058

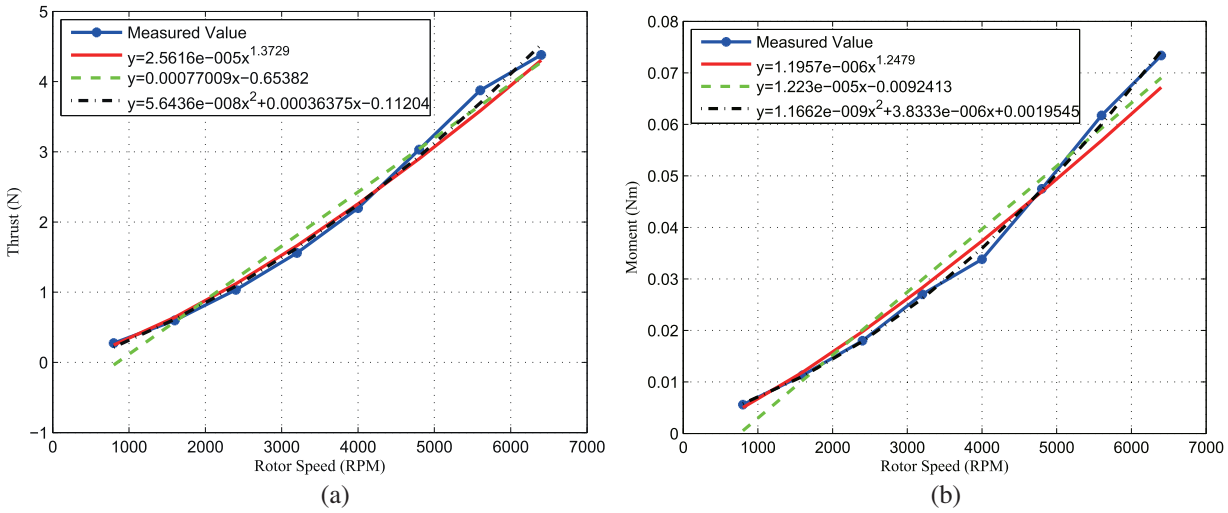

Fig. 5. The results from the parameters identification of the rotor. (a) Thrust generated by the rotor. (b) Moment generated by the rotor.

In this work, these control inputs are scaled into $[-1, 1]$, then the parameters for (25) is chosen as

$$k_T = 4000, \quad k_{\phi\theta} = k_\psi = 40 \tag{37}$$

with an output limitation of $1 \le \omega_i \le 8000$, which is the range of the motor's rotary speed.

With the parameter assignments in (37), the parameters of the attitude controller are selected by the trial and error method as

$$k_r = 12, \quad k_a = 10 \tag{38}$$

5.1.2. Trajectory tracking control

As pointed out in Section 2, the input delays exist in the trajectory tracking control. To verify this fact and gain better understanding, extra experiments are carried out. As shown in Fig. 6(a), the thrust of the rotor is recorded when the RPM command rises from 2400 to 3200 RPM. It takes approximately 0.05 s for the rotor to increase its thrust. This means there exists transport delay between the RPM commands and the measured thrusts/torques. This fact is also verified by comparing the measured acceleration and the theoretical prediction when the quadrotor is in flight. As shown in Fig. 6(b), the theoretical prediction is calculated according to (4) when every control command U_1 is sent, and the acceleration is measured by an onboard sensor simultaneously. By relevance analysis, the time delay between the measured value and prediction is approximately 0.06 s. However, if one checks every single point in Fig. 6(b), this delay is not fixed. All of these results domonstrate the effectiveness of (5).

To identify the aerodynamical drag force in (4), aerodynamic analysis [32] is utilized, where the reference area is estimated by imaging processing. The constant k_x, k_y, k_z in (4) are determined to be 0.017.

With these identified results and the developed attitude controller, control gains of the trajectory tracking controller are selected by the trial and error method as

$$c_{1p} = 2, \quad c_{1i} = 0.05, \quad c_2 = 5, \quad M_w = 5 \tag{39}$$

5.2. Simulation

In this work, the performance of the proposed controllers for the quadrotor is preliminarily examined by numerical simulations in the presence of payloads, wind and rotor failures. As shown in Fig. 7, the quadrotor follows a step reference at the beginning, then

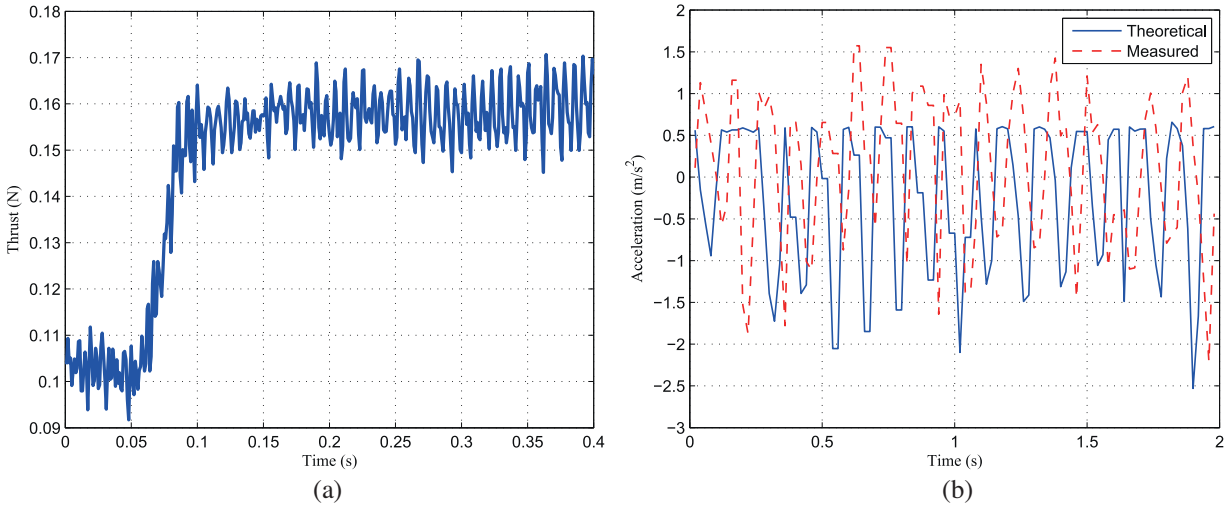

Fig. 6. A transport delay exists between the measured acceleration and theoretical predicted acceleration. (a) Transition of thrust from 2400 RPM to 3200 RPM. (b) Theoretical predicted acceleration and measured acceleration.

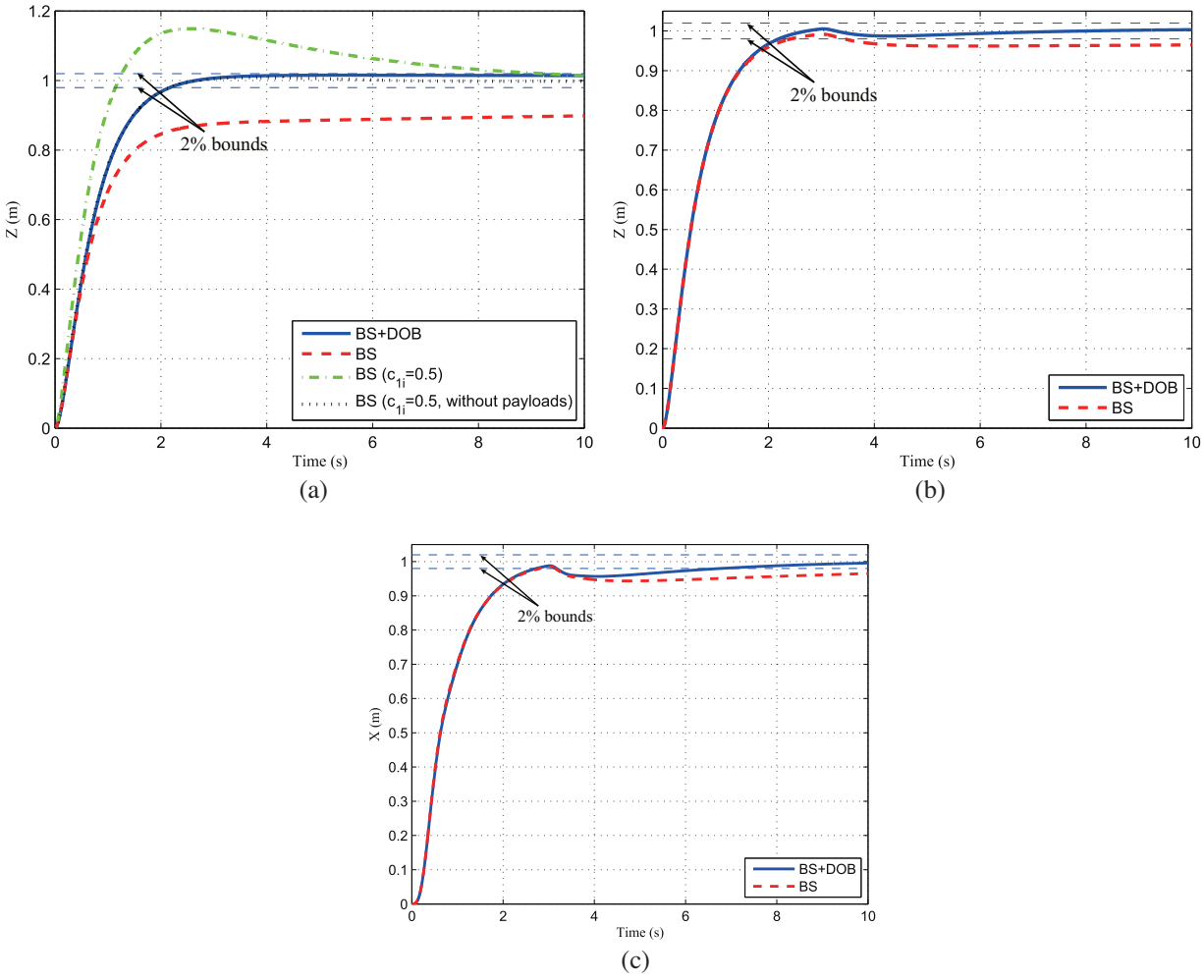

Fig. 7. Simulation results for flights under three types of disturbances. (a) Flight with 200 g payload. (b) Flight with rotor failure. (c) Flight with wind.

disturbances of different type are introduced to demonstrate the advantages of the developed DOB-based control strategy.

In Fig. 7(a), 200 g payloads are attached to the quadrotor. With the DOB, the quadrotor can be stabilized with a steady state error (SSE) of 2%, whereas the SSE of BS controller is 10%. Although increasing the integral item (c_{1i}) might be a possible way to enhance the performance of the BS control when the payloads are attached, it leads to large overshoot, even instability. As shown in Fig. 7(a), when c_{1i} increases to 0.5, the quadrotor can be well controlled with

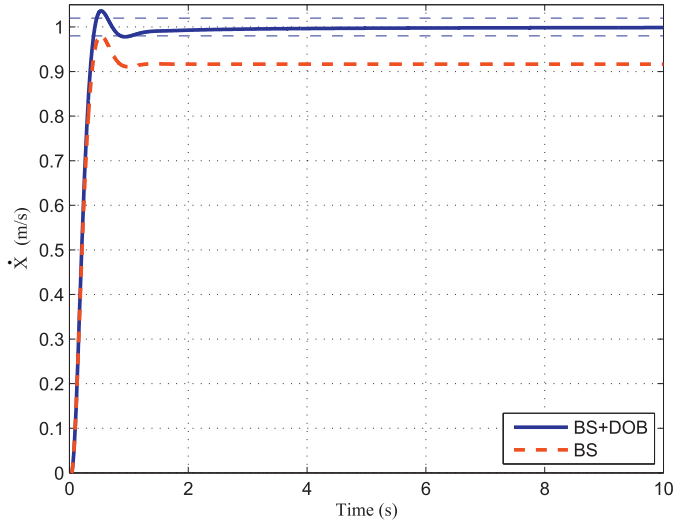

Fig. 8. Results from speed control when wind disturbances exist.

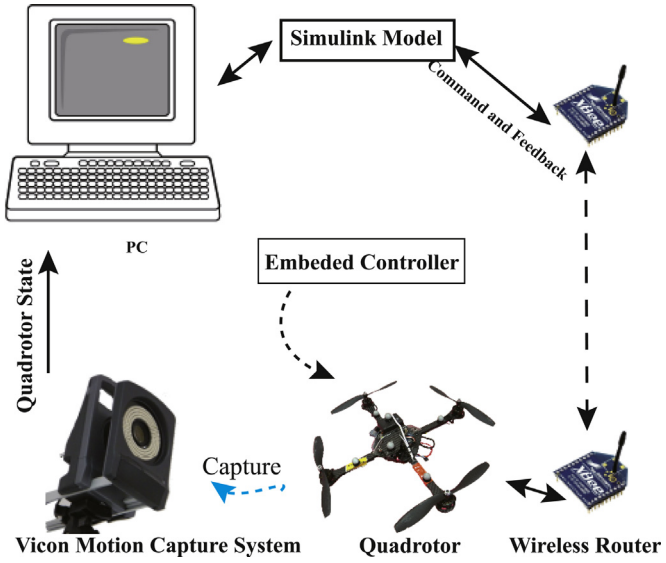

Fig. 9. The structure of an indoor test bed for the quadrotor.

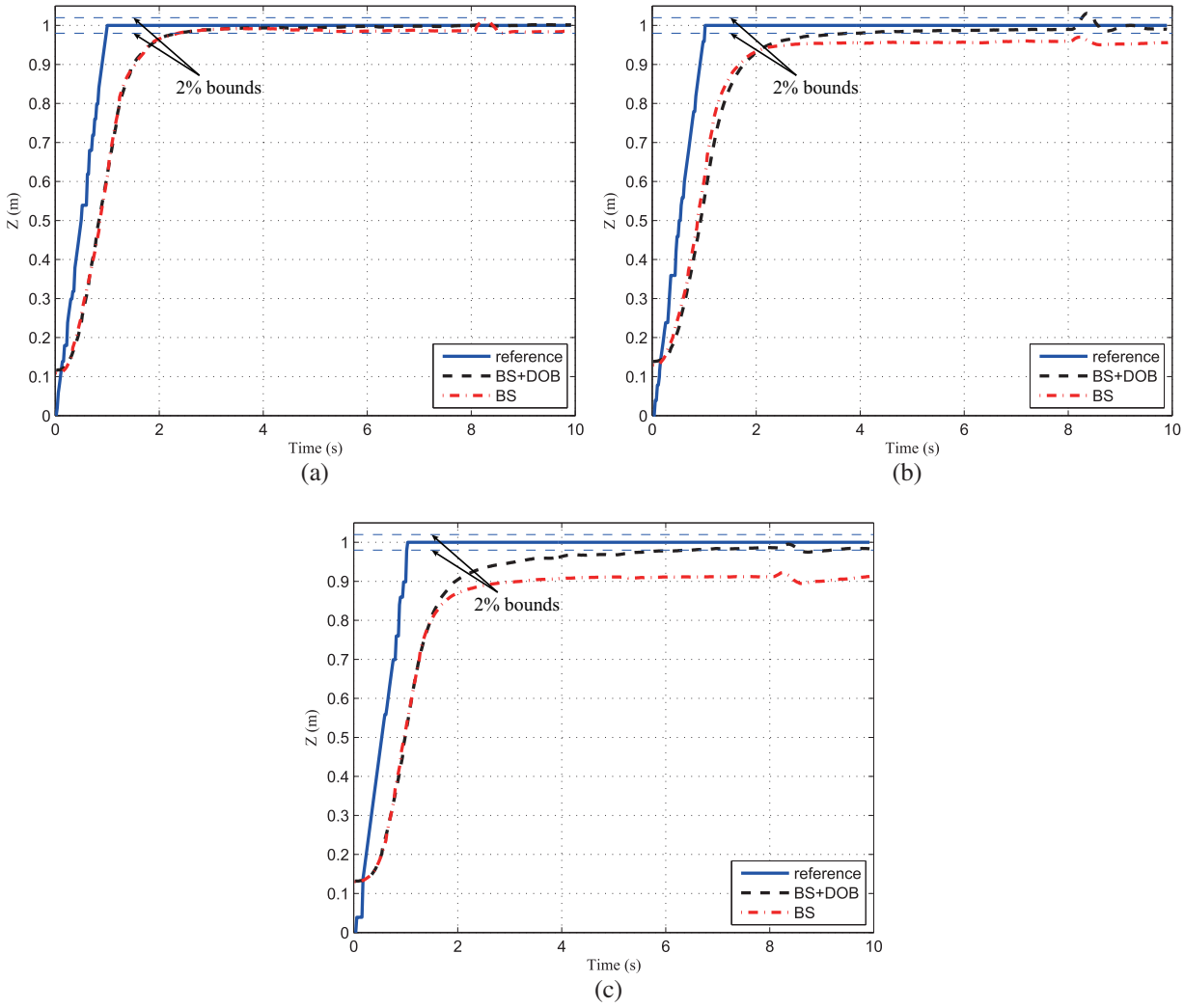

Fig. 10. Results from altitude control when the quadrotor carrying three types of payloads. (a) Altitude control with 50 g payload. (b) Altitude control with 100 g payload. (c) Altitude control with 200 g payload

the 200 g payloads. However, when this payload is removed, the overshoot for this control increases up to 15%.

In Fig. 7(b), 5% of the collective thrust of the rotors is reduced at t =3 s. When t<3 s, there is no difference between the BS controller and its counterpart. However, when t>3 s, with BS controller, the quadrotor quickly drops down and cannot be stabilized with a SSE <2%. In contrast, with DOB, the quadrotor is well controlled with a SSE of 2% in the whole process.

In Fig. 7(c), wind with the speed of 4 m/s is introduced in the negative direction of the X axis at t =3 s. Both of these two controllers quickly moves towards the negative axis direction. However, the DOB-based controller can stabilize the quadrotor with a SSE of 2% within approximately 3 s, which cannot be achieved by the BS controller.

Considering the fact that the speed control is also important in the long distance flight, an additional simulation is carried out to verify the performance of the speed controller. As shown in Fig. 8, wind with the speed of 4 m/s is introduced in the negative direction of the X axis. Without the DOB, the speed controller shows a SSE of 8%. With the use of the

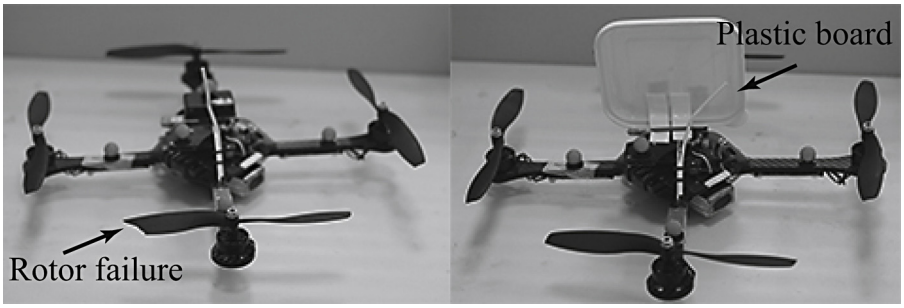

Fig. 11. About 20% of a rotor is cut off to present the disturbance of rotor failure (left), and a plastic board is vertically set up on the top of the quadrotor to amplify the disturbance of wind (right).

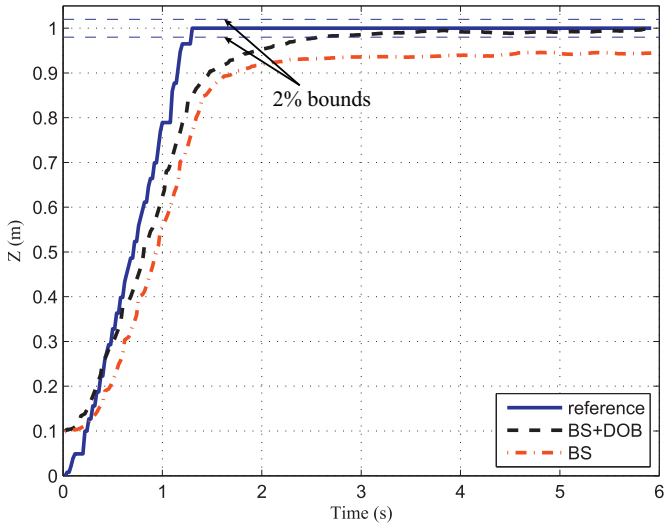

Fig. 12. Altitude control with rotor failure.

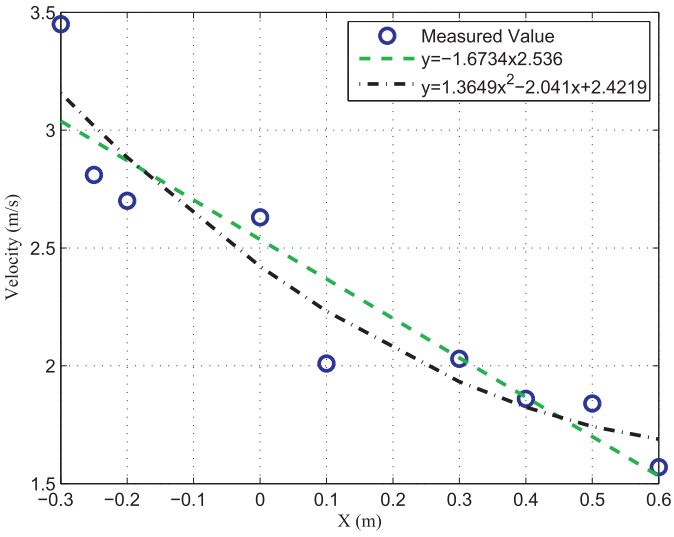

Fig. 13. The velocity of wind from the electric fan.

DOB, the speed can be controlled to its desired value within 1 s.

All of these results indicate that the proposed control strategy can effectively compensate for the lumped disturbance in the trajectory tracking, thus provides better performances.

5.3. Experimental results

Three comparative experiments are carried out to verify the effectiveness of the proposed control strategy. Payloads, rotor failures and wind are presented as different sources of disturbances.

5.3.1. Test bed

All of the experiments are conducted in an indoor test bed. As shown in Fig. 9, the quadrotor test bed is comprised of a Hummingbird quadrotor, a pair of XBee wireless routers, a control station, and a Vicon motion capture system. The quadrotor communicates with the control station via a couple of wireless routers at a frequency of 50 Hz. The control station runs on a Windows operating system. It fetches the position information of the quadrotor from the data server of the Vicon motion capture system and sends them to the quadrotor. The motion capture system runs at a frequency of 200 Hz and estimates the state of the quadrotor by kinematic fitting the reflective markers which are attached on the quadrotor.

5.3.2. Flight with payloads

As shown in Fig. 10, experimental results of the altitude control with different payloads are depicted. It can be observed that there is only a slight difference between the DOB-based controller and its counterpart when the payload is 50 g. However, as the payload increases, the DOB-based controller shows its benefits. The SSE of the traditional BS controller is 4% when the payload is 100 g, and 10% when the payload is 200 g. By contrast, the quadrotor can always be stabilized by the DOB-based controller with a SSE of 2%. An addition experiment shows that without payloads the altitude can be stabilized with a SSE <2 cm within 2 s, which is good enough for the quadrotor to fulfill most of its activities.

It can be concluded that the DOB-based controller enables the quadrotor to take flights with various payloads, and still guarantee the accuracy of trajectory tracking. It also indicates that the controller can effectively compensate for the model mismatches on the mass of the quadrotor.

5.3.3. Flight with rotor failures

As shown in the left of Fig. 11, one rotor is artificially cut off for about 20%. With this damaged rotor, it is interesting to see that the translational motion can still be well stabilized by both the BS controller and DOB-based controller. This can be explained as follows. According to (4), the control inputs for the translational motion are the collective thrust and the attitude. When the rotor gets damaged, although the gain in the attitude control and collective thrust decreases, this can be compensated by the nonlinear trajectory tracking controller. Therefore, the results from the DOB-based controller and the BS controller are nearly the same.

In the altitude control, the rotor failure equivalently increases the effects of gravity. Therefore, different results are observed as shown in Fig. 12. Similar to the behaviors in the flight with payloads, the quadrotor is unlikely to reach the desired altitude by merely BS controller. However, by implementing the DOB, the quadrotor can be stabilized with a SSE of 2% within 2.5 s.

It can be seen that the DOB-based controller is less sensitive to the tolerances of the rotor model comparing to the traditional nonlinear controllers. Therefore, it can guarantee a safe flight even if part of its thrust is lost.

5.3.4. Flight with wind disturbance

In order to artificially create the wind disturbances, an electric fan is set up at $(-0.6, 0, 0.85)$ and faces to the positive direction of the X axis. The velocity of its generated wind is then measured by a ventilation meter (TSI VelociCalc 9535) along the X axis for every 0.1 m. At each position, the measurement takes 1 min. The results are shown in Fig. 13. By quadratic fitting, the velocity of the wind can be estimated by

$$V_w = 1.4x^2 - 2.0x + 2.4 \tag{40}$$

with $V_w(-0.25) \approx 2.8$ m/s.

As the wind from the fan is relatively slow, a plastic board with size of $12.5 \times 12.5\,\text{cm}^2$ is attached on the top of the quadrotor to amplify this disturbance, as shown in the right of Fig. 11. With this configuration, the aerial drag force is nearly doubled for the quadrotor.

In the comparative experiments, the quadrotor follows a ramp reference as shown in Fig. 14. With the DOB, the response is slightly faster than that of BS, and can be stabilized with a SSE of 2% within approximately 2 s. By contrast, the SSE of the BS controller is about 5%. In addition, the DOB-based controller shows less vibrations in the steady state.

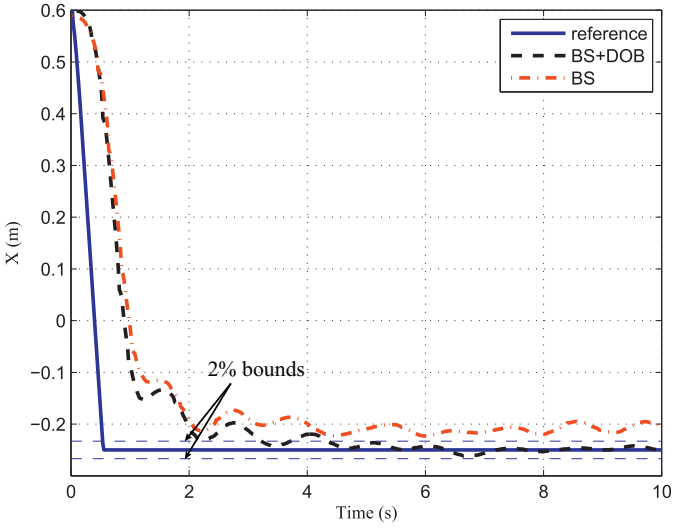

Fig. 14. Translational motion control with disturbance of wind.

All of the above experiments imply the proposed control strategy can handle the model mismatches and external disturbances very well, thus show better performance than traditional nonlinear controllers.

6. Conclusion

This paper has developed a high-performance trajectory tracking control strategy for a quadrotor and experimentally verified its performance. Based on theoretical analysis and experiments, the quadrotor model is developed by taking model mismatches, external disturbances and input delays into consideration. A DOB-based control strategy is then developed based on this model, and the stability analysis confirms its input-to-state stability. Finally, extensive simulations and experiments are carried out. The results show that the quadrotor can be stabilized with a steady state error of 2% in the presence of payloads, rotor failures and wind disturbances. It demonstrates that the robustness of the quadrotor is greatly enhanced comparing to the traditional nonlinear control technique.

Acknowledgements

This work was supported by Open Research Foundation of State Key Lab. of Digital Manufacturing Equipment & Technology in Huazhong University of Science & Technology under Grant No. DMETKF2014004.

References

[1] N. Michael, D. Mellinger, Q. Lindsey, V. Kumar, The grasp multiple micro-uav testbed, IEEE Robot. Automat. Mag. 17 (3) (2010) 56–65.
[2] H. Ramirez-Rodriguez, V. Parra-Vega, A. Sanchez-Orta, O. Garcia-Salazar, Robust backstepping control based on integral sliding modes for tracking of quadrotors, J. Intell. Robot. Syst. 73 (2014) 51–66.
[3] K. Chee, Z. Zhong, Control, navigation and collision avoidance for an unmanned aerial vehicle, Sensors Actuat. A: Phys.
[4] J. Escareño, S. Salazar, H. Romero, R. Lozano, Trajectory control of a quadrotor subject to 2d wind disturbances, J. Intell. Robot. Syst. 70 (1-4) (2013) 51–63.
[5] V. Kumar, N. Michael, Opportunities and challenges with autonomous micro aerial vehicles, in: International Symposium on Robotics Research, 2011.
[6] S. Bouabdallah, A. Noth, R. Siegwart, Pid vs lq control techniques applied to an indoor micro quadrotor, in: Proceedings of the IEEE/RSJ International Conference on Intelligent Robots and Systems, 2004 (IROS 2004), vol. 3, IEEE, 2004, pp. 2451–2456.
[7] S. Bouabdallah, Design and control of Quadrotors with Application to Autonomous Flying, 2007 (Ph.D. thesis).
[8] H. Lim, J. Park, D. Lee, H. Kim, Build your own quadrotor: Open-source projects on unmanned aerial vehicles, IEEE Robot. Automat. Mag. 19 (3) (2012) 33–45.
[9] A. Tayebi, S. McGilvray, Attitude stabilization of a vtol quadrotor aircraft, IEEE Trans. Control Syst. Technol. 14 (3) (2006) 562–571.
[10] Y. Zhang, K. Kondak, T. Lu, J. Du, M. Bernard, G. Wang, Development of the model and hierarchy controller of the quad-copter, Proc. Inst. Mech. Engrs. Part G: J. Aerospace Eng. 222 (1) (2008) 1–12.
[11] Z.T. Dydek, A.M. Annaswamy, E. Lavretsky, Adaptive control of quadrotor uavs: a design trade study with flight evaluations.
[12] F. Chen, F. Lu, B. Jiang, G. Tao, Adaptive compensation control of the quadrotor helicopter using quantum information technology and disturbance observer, J. Franklin Inst.
[13] X. Zhang, Y. Zhang, Fault tolerant control for quad-rotor uav by employing Lyapunov-based adaptive control approach, in: AIAA Guidance, Navigation, and Control Conference, 2010, pp. 2–5.
[14] A. Chamseddine, Y. Zhang, C.-A. Rabbath, C. Fulford, J. Apkarian, Model reference adaptive fault tolerant control of a quadrotor uav, in: Proceedings of AIAA InfoTech@ Aerospace 2011: Unleashing Unmanned Systems, 2011, pp. 29–31.
[15] L. Besnard, Y.B. Shtessel, B. Landrum, Quadrotor vehicle control via sliding mode controller driven by sliding mode disturbance observer, J. Franklin Inst. 349 (2) (2012) 658–684.
[16] X. Chen, J. Li, J. Yang, S. Li, A disturbance observer enhanced composite cascade control with experimental studies, Int. J. Control Automat. Syst. 11 (3) (2013) 555–562.
[17] Z.-J. Yang, S. Hara, S. Kanae, K. Wada, C.-Y. Su, An adaptive robust nonlinear motion controller combined with disturbance observer, IEEE Trans. Control Syst. Technol. 18 (2) (2010) 454–462.
[18] L. Besnard, Y.B. Shtessel, B. Landrum, Control of a quadrotor vehicle using sliding mode disturbance observer, in: American Control Conference, 2007, ACC'07, IEEE, 2007, pp. 5230–5235.
[19] A. Benallegue, A. Mokhtari, L. Fridman, High-order sliding-mode observer for a quadrotor uav, Int. J. Robust Nonlinear Control 18 (4–5) (2008) 427–440.
[20] R. Zhang, Q. Quan, K.-Y. Cai, Attitude control of a quadrotor aircraft subject to a class of time-varying disturbances, IET Control Theory Applicat. 5 (9) (2011) 1140–1146.
[21] S.-H. Jeong, S. Jung, Experimental studies of a disturbance observer for attitude control of a quad-rotor system, in: 12th International Conference on Control, Automation and Systems (ICCAS), 2012, IEEE, 2012, pp. 579–583.
[22] Z. Cen, H. Noura, Y.A. Younes, Robust fault estimation on a real quadrotor uav using optimized adaptive thau observer, in: International Conference on Unmanned Aircraft Systems (ICUAS), 2013, IEEE, 2013, pp. 550–556.
[23] D.J. Zhao, B.Y. Jiang, Robust attitude control of quadrotor vehicle via extended state observer, Appl. Mech. Mater. 373 (2013) 1445–1448.
[24] M. Abdolhosseini, Y. Zhang, C. Rabbath, An efficient model predictive control scheme for an unmanned quadrotor helicopter, J. Intell. Robot. Syst. (2012) 1–12.
[25] S. Bouabdallah, R. Siegwart, Full control of a quadrotor, in: IEEE/RSJ International Conference on Intelligent Robots and Systems, 2007, IROS 2007, IEEE, 2007, pp. 153–158.
[26] W. Dong, G. Gu, X. Zhu, H. Ding, Modeling and control of a quadrotor uav with aerodynamic concepts, in: ICIUS 2013: International Conference on Intelligent Unmanned Systems, 2013.
[27] S. Bouabdallah, P. Murrieri, R. Siegwart, Design and control of an indoor micro quadrotor, in: Proceedings of the IEEE International Conference on Robotics and Automation, 2004, ICRA'04, vol. 5, IEEE, 2004, pp. 4393–4398.
[28] D. Mellinger, V. Kumar, Minimum snap trajectory generation and control for quadrotors, in: IEEE International Conference on Robotics and Automation (ICRA), 2011, IEEE, 2011, pp. 2520–2525.
[29] B. Yao, M. Al-Majed, M. Tomizuka, High-performance robust motion control of machine tools: an adaptive robust control approach and comparative experiments, IEEE/ASME Trans. Mechatron. 2 (2) (1997) 63–76.
[30] J.-H. Park, G.-T. Park, Adaptive fuzzy observer with minimal dynamic order for uncertain nonlinear systems, IEE Proc-Control Theory Applicat. 150 (2) (2003) 189–197.
[31] Z.-J. Yang, H. Tsubakihara, S. Kanae, K. Wada, C.-Y. Su, A novel robust nonlinear motion controller with disturbance observer, IEEE Trans. Control Syst. Technol. 16 (1) (2008) 137–147.
[32] J. Leishman, Principles of Helicopter Aerodynamics, Cambridge University Press, New York, 2006.
[33] M. Hehn, R. D'Andrea, A flying inverted pendulum, in: IEEE International Conference on Robotics and Automation (ICRA), 2011, IEEE, 2011, pp. 763–770.

Biographies

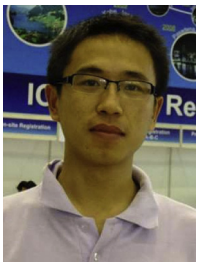

Wei Dong received the B.E. degree (with honors) in mechanical engineering from Shanghai Jiao Tong University, Shanghai, China, in 2009, where he is currently pursuing the Ph.D. degree in mechanical engineering. His research interest is on the modeling and control of unmanned aerial vehicles.

Guo-Ying Gu received the B.E. degree (with honors) in electronic engineering and the Ph.D. degree (with honors) in mechanical engineering from Shanghai Jiao Tong University, Shanghai, China, in 2006 and 2012, respectively. Dr. Gu is currently working as a postdoctoral research fellow with School of Mechanical Engineering at Shanghai Jiao Tong University. He was a Visiting Researcher with Department of Mechanical and Industrial Engineering at Concordia University, Montreal, QC, Canada from October 2010 to March 2011 and from November 2011 to March 2012. His research interests include modeling and control of smart material based actuators with hysteresis, high-bandwidth motion control of nanopositioning stages, and control of unmanned aerial vehicles.

Xiangyang Zhu received the B.S. degree from the Department of Automatic Control Engineering, Nanjing Institute of Technology, Nanjing, China, in 1985, the M.Phil. degree in instrumentation engineering and the Ph.D. degree in automatic control engineering, both from Southeast University, Nanjing, China, in 1989 and 1992, respectively. From 1993 to 1994, he was a postdoctoral research fellow with Huazhong University of Science and Technology, Wuhan, China. He joined the Department of Mechanical Engineering as an associate professor, Southeast University, in 1995. Since June 2002, he has been with the School of Mechanical Engineering, Shanghai Jiao Tong University, Shanghai, China, where he is currently a Changjiang Chair Professor and the director of the Robotics Institute. His current research interests include robotic manipulation planning, human-machine interfacing, and biomechatronics. Dr. Zhu received the National Science Fund for Distinguished Young Scholars in 2005.

Han Ding received his Ph.D. degree from Huazhong University of Science and Technology (HUST), Wuhan, China, in 1989. Supported by the Alexander von Humboldt Foundation, he was with the University of Stuttgart, Germany from 1993 to 1994. He worked at the School of Electrical and Electronic Engineering, Nanyang Technological University, Singapore from 1994 to 1996. He has been a Professor at HUST ever since 1997 and is now Director of State Key Lab of Digital Manufacturing Equipment and Technology there. Dr. Ding was a "Cheung Kong" Chair Professor of Shanghai Jiao Tong University from 2001 to now. Dr. Ding acted as an Associate Editor of IEEE Trans. on Automation Science and Engineering(TASE) from 2004 to 2007. Currently, he is an Editor of IEEE TASE and a Technical Editor of IEEE/ASME Trans. on Mechatronics. His research interests include robotics, multi-axis machining and control engineering.